Hapres | Journal of Sustainability Research

sustainability.hapres.com

Article

Q_{cycle}: A Field-Robust Metric for $LiFePO_4$ Battery Degradation Monitoring in Sahelian Solar Irrigation Systems

Amadou Keïta [1,*], Daniel Yamegueu [2], Sodiya Keïta [2], Djim Doumbe Damba [1]

[1] Laboratoire Eaux, Hydro-Systèmes et Agriculture (LEHSA), Institut International d'Ingénierie de l'Eau et de l'Environnement (Institut 2iE), Rue de la Science, Ouagadougou 01 BP 594, Burkina Faso; djim.damba@2ie-edu.org (DDD)

[2] Laboratoire Énergies Renouvelables et Efficacité Énergétique (LabEREE), Institut International d'Ingénierie de l'Eau et de l'Environnement (Institut 2iE), Rue de la Science, Ouagadougou 01 BP 594, Burkina Faso; daniel.yamegueu@2ie-edu.org (DY); sodiya.keita@2ie-edu.org (SK)

* Correspondence: Amadou Keïta, Email: amadou.keita@2ie-edu.org; Tel.: +226-68-768-801.

ABSTRACT

Solar-powered irrigation is expanding across the Sahel, yet a lack of field-compatible health metrics for $LiFePO_4$ batteries limits predictive maintenance in decentralized systems. Coulombic Efficiency (*CE*) is unreliable under natural temperature and humidity fluctuations, thus masking early degradation. This study introduces Q_{cycle}, the total capacity per charge-discharge cycle ($Q_C + Q_D$), and validates its robustness relative to *CE* under Sahelian semi-field conditions. Four 280 Ah $LiFePO_4$ cells were cycled over five months (May–September 2022) in Kamboinsé, Burkina Faso, spanning dry and rainy seasons. Two regimes represented agricultural use: rapid 24-h cycles (146 total) and slow 96-h cycles (35 total). While *CE* oscillated erratically, Q_{cycle} revealed consistent exponential capacity fade. Nonlinear regression yielded high goodness-of-fit values (R^2 = 0.97 to 0.99), demonstrating the ability of Q_{cycle} to consistently capture the observed degradation trend across the tested cells and cycling regimes. Q_{cycle} provides a practical, instrumentation-tolerant alternative to *CE* for decentralized solar irrigation, supporting predictive maintenance in the water-energy-food nexus and advancing SDG 7 targets.

KEYWORDS: battery health monitoring; $LiFePO_4$ degradation; Q_{cycle} metric; Sahelian climate; solar irrigation; water–energy–food nexus

Received: 22 May 2026
Accepted: 31 Jul 2026
Published: 04 Aug 2026

ABBREVIATIONS

2iE, Institut International d'Ingénierie de l'Eau et de l'Environnement; AC, alternating current; BESS, battery energy storage system; BMS, battery management system; *CE*, Coulombic efficiency; CPU, central processing unit; d*Q*/d*V*, differential capacity analysis; EB Tester, battery testing

software; F1/F2, first and second principal components; LA, lead-acid; LabEREE, Laboratoire Énergies Renouvelables et Efficacité Énergétique; LEHSA, Laboratoire Eaux, Hydro-Systèmes et Agriculture; $LiCoO_2$, lithium cobalt oxide; $LiFePO_4$, lithium iron phosphate; Li-ion, lithium-ion; *MSE*, mean squared error; N_{cycle}, total number of cycles; OCV, open-circuit voltage; PCA, principal component analysis; PV, photovoltaic; Q_C, charged capacity; Q_D, discharged capacity; Q_{cycle0}, initial cycle capacity; $Q_{cyclemin}$, end-of-life cycle capacity threshold; R-cells, rapid cycling scenario cells; *RH*, relative humidity; *RMSE*, root mean squared error; S-cells, slow cycling scenario cells; SDG, Sustainable Development Goal; SEI, solid electrolyte interphase; SoC, state of charge; SoH, state of health; USB, universal serial bus; V_{max}, maximum charging voltage; V_{min}, minimum discharging voltage

INTRODUCTION

Study Background

Does sustainable development in the Sahel require integrated approaches to the water-energy-food nexus [1]. Agriculture employs more than 60% of the working population in Sahelian countries and accounts for up to 50% of GDP when livestock is included [2,3], yet productivity remains constrained by unreliable rainfall and limited irrigation infrastructure.

Solar-powered irrigation provides a promising pathway toward sustainable agricultural intensification, aligning with Sustainable Development Goal 7 (affordable and clean energy) [4,5] and SDG 2 (zero hunger). However, the long-term viability of such systems depends on durable energy storage. While lithium iron phosphate ($LiFePO_4$) batteries are increasingly used in off-grid solar applications, their degradation behavior under harsh Sahelian conditions is still poorly understood, and standard indicators such as Coulombic Efficiency (*CE*) are highly sensitive to the temperature and humidity fluctuations inherent to field environments.

This study addresses this gap by introducing Q_{cycle}, the total capacity per charge-discharge cycle, and demonstrating its robustness relative to *CE* under Sahelian semi-field conditions. By linking electrochemical engineering with agricultural sustainability, this research contributes to the food nexus literature and supports evidence-based decisions for the rural energy transition.

Research Question and Objectives

Despite the growing deployment of $LiFePO_4$ batteries in solar irrigation, field-compatible health metrics remain lacking. *CE*, widely used in laboratory settings, becomes erratic amid natural environmental shifts, masking early degradation. This finding raises three questions: (1) How reliably can *CE* track degradation compared to Q_{cycle} in decentralized semi-field Sahelian conditions? (2) What capacity-fade patterns does Q_{cycle}

reveal under rapid versus slow agricultural cycling regimes? (3) What cell-level lifespan can theoretically be projected from Q_{cycle} decay, and how does manufacturing heterogeneity influence these projections?

The overall aim was to advance sustainable energy storage practices in the Sahel by validating Q_{cycle} as a practical, instrumentation-tolerant alternative to *CE*. Unlike empirical lifetime prediction models, the objective of the present work was primarily to introduce and validate a reliable degradation monitoring metric (Q_{cycle}) under semi-field operating conditions. Lifespan projection was explored only as one possible application of the degradation trajectories derived from this metric. The specific objectives were to quantify degradation rates across two realistic operating scenarios, model capacity fade via nonlinear regression, and estimate theoretical cell lifespans for decentralized solar irrigation systems.

MATERIALS AND METHODS

Experimental Setup and Materials

A redundant experimental setup was implemented to ensure reliable battery testing under unstable electricity-supply conditions common in the Sahel (Figure 1). The system was initially powered by the national electricity grid (220 V AC) managed by SONABEL. Anticipating frequent outages, two additional backup levels were added to maintain uninterrupted operation. A 5.5 kW generator served as the primary backup source, while an automatic switch ensured a seamless transition between grid power and generator (Figure 1, ①). As an intermediate safeguard, a hybrid converter with integrated backup batteries supplied energy during brief outages (Figure 1, ②). A third backup layer was added through a SATGTAG inverter (3 kVA/2400 W), providing up to 30 min of autonomy (Figure 1, ③). These safeguards were implemented after preliminary commissioning tests, which showed that sudden power interruptions could cause data loss in the EB Tester software. During the reported five-month experiment, however, no data loss or cycle interruption occurred; consequently, no data interpolation or reconstruction was required.

Battery testing was conducted using four ZKETECH A40L battery testers (T1 to T4), each connected to a dedicated $LiFePO_4$ cell (R1, R2, S1, or S2) and to a separate computer (CPU1 to CPU4). Each computer ran the EB Tester Software (version 5.1), which managed test programming, real-time data display, and time-step recording (Figure 1, ④). A multimeter was used to cross-check voltage and current values from the testers each week, ensuring measurement accuracy. Ambient temperature and relative humidity were recorded continuously throughout the experiment using a TempU08B USB data logger [6], with sensors positioned adjacent to the battery cells to record representative environmental conditions.

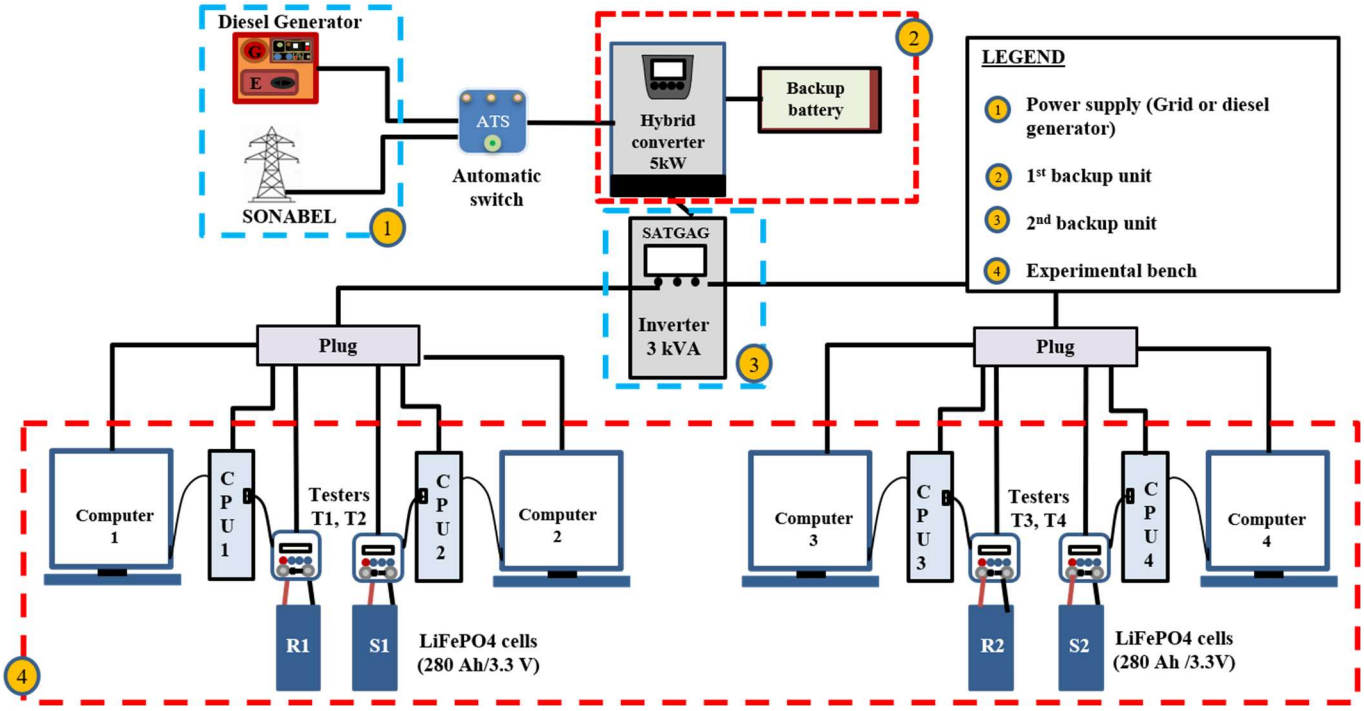

Figure 1. Experimental setup diagram. The system integrates three levels (①, ②, ③) of backup power supply (grid, generator, inverter) to ensure data continuity. Four ZKETECH A40L testers (④) (T1–T4) are connected to $LiFePO_4$ cells (R1, R2, S1, S2) and to computers (CPU1–CPU4) running the EB Tester software. Environmental conditions are logged using a USB data logger (TempU08B).

Battery Cells and Test Protocols

Four 280 Ah/3.2 V lithium iron phosphate ($LiFePO_4$) prismatic cells were tested continuously for five months (May–September 2022), covering both dry and rainy seasons in Kamboinsé, Burkina Faso (latitude 12°26'48" N, longitude 1°33'45" W). The cells had the same brand, capacity, and batch, with assumed uniform initial characteristics. Given the absence of manufacturer datasheets, nominal cell characteristics were compiled from peer-reviewed literature (Table 1). The values for nominal voltage, open-circuit voltage (OCV), and cutoff thresholds were aligned with prior experimental studies on 280 Ah class $LiFePO_4$ cells under similar operating conditions [7].

Table 1. Design parameters for the $LiFePO_4$ cells evaluated in this study.

Parameter	Assumed value	Justification
Cell capacity	280 Ah	Stated on battery casing (manufacturer label)
Nominal voltage	3.2 V	Stated on battery casing
Maximum charging voltage (V_{max})	3.65 V	Standard for LFP chemistry
Minimum discharging voltage (V_{min})	3.00 V	Common cutoff to avoid over-discharge
Open-circuit voltage (OCV)	3.30 V	Typical for $LiFePO_4$ cells at 100% SoC

Two realistic operating scenarios were used based on local solar energy use profiles in Burkina Faso [8]: (i) a “fast” scenario simulating high daily energy turnover (Scenario R), and (ii) a “slow” scenario simulating extended storage and moderate consumption (Scenario S). In the fast

scenario, each charge/discharge cycle spanned 24 h, with charging set to 8 h to represent the average daily sunshine duration [9,10], and discharging lasting 16 h to represent nighttime irrigation operation. Charging and discharging currents were $I_{R\text{-}charge}$ = 35.76 A and $I_{R\text{-}discharge}$ = 17.87 A, corresponding to C-rates of 0.13C and 0.064C, respectively, which reflected the energy demand of a typical 2.2 kW/220 V submersible pump (flow rate ≈ 5 m^3/h; total head = 75 m) that is commonly used to irrigate 1.0 hectare of farmland [11].

In the slow scenario (Scenario S), each cycle spanned 96 h (4 days), with a charging period of 32 h and a discharging period of 64 h, representing cloudy weather or low usage. The charging and discharging currents were $I_{S\text{-}charge}$ = 8.79 A and $I_{S\text{-}discharge}$ = 4.39 A, corresponding to C-rates of 0.031C and 0.016C, respectively. These values are consistent with current levels used in domestic solar installations deployed by the national utility in rural Burkina Faso [12]. All tests used constant-current charging and discharging modes, with voltage and current values checked once a week with an independent multimeter to ensure accuracy.

Novel Degradation Metric: Q_{cycle}

This study introduces Q_{cycle} as a new indicator for monitoring battery degradation under field conditions. Coulombic Efficiency (*CE*), which is defined as the ratio of discharged to charged capacity (1):

$$CE = Q_C/Q_D \quad (1)$$

is widely used but suffers from high sensitivity to measurement errors [13,14]. To overcome these limitations, Q_{cycle} was defined as the total capacity exchanged during each cycle (2):

$$Q_{cycle} = Q_C + Q_D \quad (2)$$

where Q_C (Ah) is the charged capacity and Q_D (Ah) is the discharged capacity within the same cycle.

Because this metric adds rather than divides two measured quantities, it provides a more stable and reliable signal in real-world conditions where small instrumental variations occur. To demonstrate this advantage, consider a typical case where the charged capacity (Q_C) is 50 Ah with an uncertainty of ±1 Ah, and the discharged capacity (Q_D) is 49 Ah with equal uncertainty. The resulting *CE* is 49/50 = 0.98 (98%). However, due to measurement uncertainty, Q_D may range from 48 to 50 Ah, and Q_C from 49 to 51 Ah. This yields extreme *CE* values of 48/51 ≈ 94.1% and 50/49 ≈ 102.0%, which results in potential variability of ±4% around the nominal value. In contrast, the corresponding Q_{cycle} is 50 + 49 = 99 Ah, with a combined propagated uncertainty of ±2 Ah, yielding a relative error of ±2.0%. This example demonstrates that Q_{cycle}, by avoiding division, is less sensitive to small variations in input data and produces a more stable signal for long-duration monitoring under semi-field conditions (Table 2).

In practical photovoltaic irrigation systems, partial charging and discharging events are expected due to variable solar irradiance and fluctuating pumping demand. In such situations, Q_{cycle} should be summed over successive partial events until one equivalent full charge-discharge cycle is completed, in line with the widely adopted concept of Equivalent Full Cycles (EFC) in battery management [15,16]. With this implementation, temporary declines in daily charge throughput reflect operational conditions rather than intrinsic battery degradation, which allows Q_{cycle} to remain representative of the available cell capacity.

In a Battery Management System (BMS), this implementation requires only continuous accumulation of charged and discharged ampere-hour throughput values, which are routinely measured by coulomb-counting algorithms. Once the cumulative throughput reaches one Equivalent Full Cycle (EFC), Q_{cycle} can be updated without extra sensors or computationally intensive diagnostics. This makes the proposed metric compatible with existing BMS architectures for long-term field monitoring.

Other state-of-health (SoH) indicators (Table 2), including differential capacity (dQ/dV), entropy profiling, and voltage relaxation are commonly used in laboratory settings to detect subtle degradation mechanisms in lithium-ion batteries at high precision [17–19]. However, these methods typically rely on high-frequency voltage measurements, precise thermal regulation, or long rest periods between cycles, which makes them less compatible with long-duration studies conducted in naturally variable environments. Likewise, while the total number of charge/discharge cycles (N_{cycle}) is a widely used metric for comparing technologies (Table 3), particularly between Li-ion and lead-acid systems [20,21] offer little insight into partial cycling, energy throughput, or efficiency losses.

As summarized in Table 2, this study presents Q_{cycle} as a practical and stable alternative, especially suited to long-term diagnostics under real-world conditions. Recent studies indicate that battery health assessment increasingly relies on combining complementary indicators that capture different degradation mechanisms, including cycling, calendar, and thermal aging [23]. In this framework, Q_{cycle} is designed to complement, rather than replace, established laboratory-based diagnostic techniques. By emphasizing resistance to data noise and compatibility with uninterrupted cycling, Q_{cycle} enables reliable performance tracking without the stringent control requirements of traditional SoH metrics. This strengthens its relevance for semi-field applications in regions such as the Sahel, where reliable year-round evaluation of energy storage systems is needed to support solar-powered infrastructure.

Table 2. Battery state of health indicators.

Metric	Definition/basis	Advantages	Limitations	Suitability for Field Study
Coulombic Efficiency *(CE)*	Ratio of discharged to charged capacity (Q_D/Q_C)	Simple to compute; widely used	Sensitive to noise; error propagation through ratio; low early-stage sensitivity	Not ideal
Q_{cycle} (this study)	Sum of charged and discharged capacity ($Q_C + Q_D$)	Lower error propagation; stable across fluctuations	Less common in literature; requires contextual interpretation	Very suitable
dQ/dV (Differential Capacity)	Slope of voltage-capacity curve during cycling	Sensitive to electrochemical changes	Requires high-resolution data; sensitive to noise; unsuitable outside the laboratory	Not applicable
Entropy Profiling	Thermodynamic entropy changes during cycling	Detects subtle aging effects	Requires precise temperature control and rest periods	Not feasible
Voltage Relaxation	Voltage behavior after rest period following cycling	Reflects internal resistance growth	Requires long rest periods; frequent interruptions are not field-compatible	Not suitable
N_{cycle} (Cycle Count)	Number of full charge/discharge cycles	Easy reference metric; used in product comparisons	Ignores depth of discharge, partial cycling, and efficiency	Informative only

Table 3. Characteristics of the two most common battery technologies on the market.

Battery energy storage system (BESS)	Energy density (Wh/kg)	Self-discharge (%/month)	Efficiency (%)	Lifetime N_{cycle} (number of cycles)	Cost (€/kWh)
Lead-acid (LA)	25–45	40	60–98	300–1500	50–200
Lithium-ion (Li-ion)	80–150	20	90–100	>1500	700–1000

*Adapted from Korsaga (2018) [22].

In addition to electrochemical data, the influence of ambient temperature and relative humidity, known contributors to lithium-ion degradation, was continuously tracked using a USB data logger [24]. These environmental factors were analyzed using time-series plots, Pearson correlation analysis, and Principal Component Analysis (PCA).

All tests were conducted over a continuous five-month period, spanning both dry and rainy seasons. This duration ensured that the results reflected a realistic range of Sahelian environmental conditions. By integrating electrochemical response, environmental stressors, and operational variability, the methodology aimed to provide a reliable, field-relevant evaluation of $LiFePO_4$ battery performance in solar-powered applications.

The end-of-life criterion was defined from preliminary trials revealing that devices connected to series-connected sets of four batteries ceased operating when voltage fell below 3 V. At that point, stored energy amounted to approximately 20% of nominal capacity. Because Q_{cycle} represents approximately double the nominal capacity, the end-of-life threshold was set at $Q_{cyclemin}$ = 40% of the cell's initial cycle capacity (Q_{cycle0}), corresponding to a remaining battery capacity of approximately 80% of nominal rated capacity (SoH = 80%), a widely accepted industry standard for defining battery end-of-life.

Data Collection and Environmental Monitoring

Data were collected using EB Tester Software (version 5.1), with data extracted monthly using USB storage devices. The charged capacity Q_C (Ah) and discharged capacity Q_D (Ah) were recorded for each cycle, together with voltages and currents at the start and end of each cycle. Environmental parameters were measured using a TempU08B USB data logger configured to log temperature and relative humidity at 15-min intervals throughout the five-month testing period.

The study was conducted under semi-field conditions representative of Sahelian environments, where electricity access, ambient temperature, and humidity levels varied naturally. No artificial environmental controls or climate chamber were used; all data were collected under real ambient conditions. Temperature ranged from 26.8 °C to 40 °C, and relative humidity varied from 19% to 77.9%, reflecting typical Sahelian climatic conditions [25]. Unlike the Sahara, where extreme diurnal temperature variations cause drastic fluctuations, the Sahel experiences moderate variations with nighttime temperatures rarely dropping below 20 °C [26,27]. This distinction is important for assessing lithium-ion battery degradation, because extreme cold is not a significant concern in this region [28].

Statistical Analysis

Time Series Analysis

Time series analysis was performed using Microsoft Excel 2019 to plot trends for Coulombic Efficiency (*CE*), cycle capacity (Q_{cycle}), ambient temperature, and relative humidity. Trends were assessed visually and through descriptive statistics to identify degradation patterns and environmental effects.

Principal Component Analysis

Principal Component Analysis (PCA) was conducted using XLSTAT version 2019.2.2 [29,30] to examine relationships between time *t*, battery capacity Q_{cycle} (Ah), temperature (°C), and relative humidity (%). Data were organized with each variable as a column and each observation as a row. After the formatting was verified, the data were standardized (z-score normalization) because variables were measured on different scales, thereby ensuring comparability.

The PCA was conducted with these four variables as active variables. Eigenvalues were analyzed to determine the number of significant principal components, and components with eigenvalues greater than 1 were retained. Factor loadings were examined to identify which variables contributed the most to each principal component, indicating potential correlations and patterns of variation. Biplots and scree plots [31] were generated to visualize relationships and variations, enabling a comprehensive interpretation of the PCA results.

Nonlinear Regression Modeling

Battery lifespan was modeled using nonlinear regression and an exponential decay function applied to Q_{cycle} data over time. The model was implemented in XLSTAT version 2019.2.2 [29,30] using the following equation [32,33]:

$$Q_{cycle}(t) = Q_{c_0} * e^{(-bt)} \quad (3)$$

where Q_{cycle} (Ah) is the battery cell capacity exchanged during each cycle, Q_{c0} (Ah) is the initial cycle capacity at the start of testing, b is the decay rate constant ($b > 0$), and t (h) is time.

A defined sampling strategy supported model robustness. For R-cells (daily cycles), 30 observations were randomly selected from 140 total observations for validation, leaving 116 for model calibration. For S-cells (4-day cycles), 10 observations were randomly selected from 35 available data points for validation, leaving 25 for calibration. XLSTAT iteratively adjusted parameters to minimize differences between observed and predicted Q_{cycle} values using the Levenberg-Marquardt algorithm, providing estimates of Q_{c0} and b and their standard errors.

Goodness of fit was assessed using the coefficient of determination (R^2), mean squared error (*MSE*), and root mean squared error (*RMSE*) [34,35].

Diagnostic plots of residuals were examined to validate model assumptions and verify the model's suitability for describing the data. Lifespan projections were calculated with Excel's Goal Seek function to determine the time t corresponding to the target value Q_{cmin} (40% of Q_{c0}), with results converted from hours to years.

RESULTS

Characterization of $LiFePO_4$ Charge/Discharge Cycle Phases

The cycle curves shown in Figures 2 and 3 show distinct features in the charging and discharging behavior of the lithium-ion cells studied. In the rapid charging scenario depicted in Figure 2, the charge curve initially shows a bulk intercalation phase (1) between 3.30 and 3.40 V, during which approximately 37.25% of the cell's nominal capacity (280 Ah) is charged. This phase is followed by a first plateau intercalation phase (2) between 3.40 and 3.43 V, contributing about 23.70% of the total charge. Finally, a second slower intercalation phase (3) occurs between 3.43 and 3.44 V, in which approximately 33.55% of the capacity is added. These observations are consistent with prior studies [36,37], which report similar multi-step voltage behavior in $LiFePO_4$ chemistry associated with phase transitions and lithium staging within the cathode material.

The discharge process, as depicted in Figure 2, also consists of three phases. It begins with the first deintercalation phase (4), during which 29.61% of the capacity is discharged from the battery between 3.31 and 3.3 V. This is followed by the second deintercalation phase (5), shown by the second plateau between 3.3 and 3.25 V, during which 37.23% of the cell's capacity is removed. The final residual discharge phase (6) occurs between 3.25 and 3.10 V, during which 29.51% of the capacity is extracted. These phases are consistent with the discharge profiles described by Hu et al. (2011) [38] and Han et al. (2019) [39], who describe the distinct stages of lithium-ion battery discharge and their impact on overall battery performance and longevity.

The discharge process of the S-cells similarly has three distinct phases (Figure 3). Initially, the first deintercalation phase (4), occurring between 3.31 and 3.3 V, extracts approximately 30.46% of the battery's capacity. This pattern agrees with findings by Khairunnisa and Mafturoh (2023) [40], who report similar initial discharge characteristics in their study of lithium iron phosphate batteries under rapid cycling conditions. The second deintercalation phase (5), represented by the second plateau between 3.3 and 3.25 V, discharges an additional 37.41% of the cell's capacity. This phase is comparable to those observed in other studies [40–42], where a stable plateau region indicates efficient energy extraction during the mid-discharge cycle. Finally, the residual discharge phase (6) of the S-cells, spanning from 3.25 to 3.10 V, discharges 29.27% of the cell's capacity.

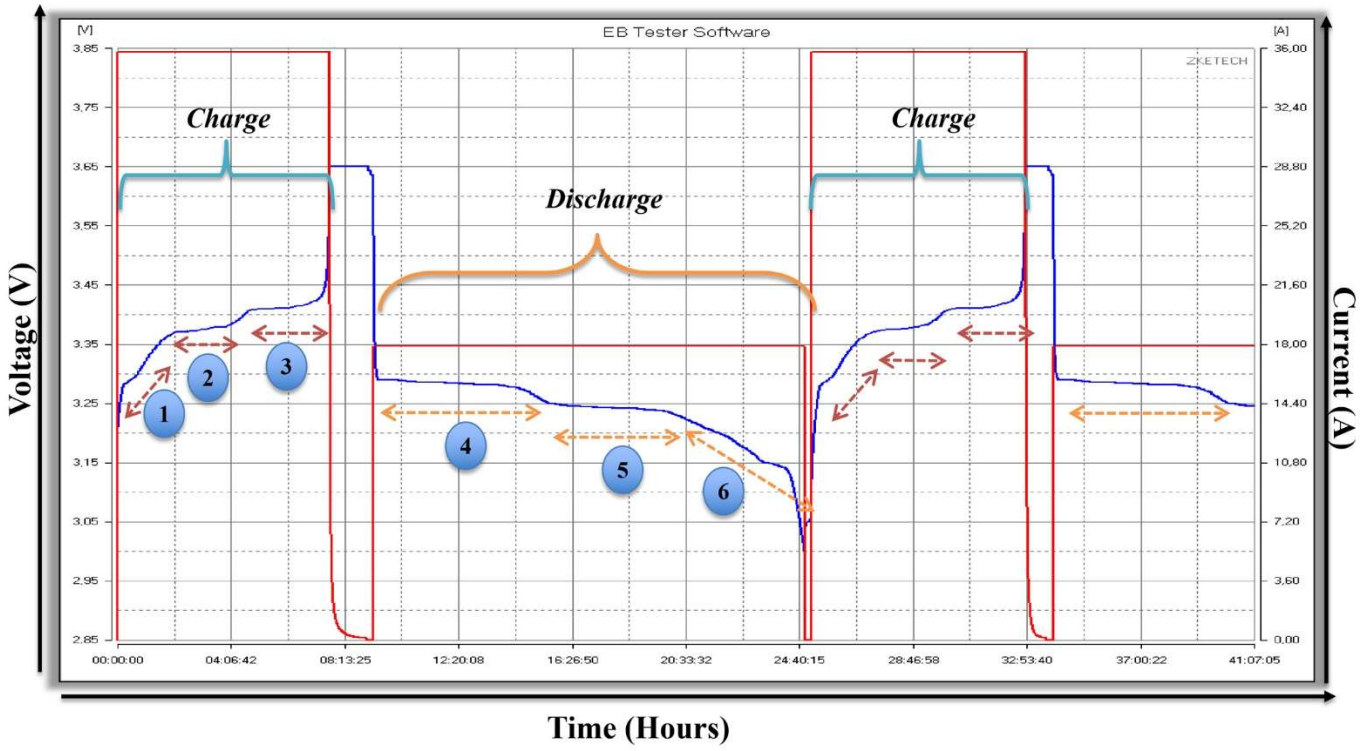

Figure 2. R-cell operating cycle under the rapid scenario. The numbers indicate the following phases: (1) raw charge phase, (2) first intercalation phase, (3) second intercalation phase, (4) first deintercalation phase, (5) second deintercalation phase, (6) residual discharge phase.

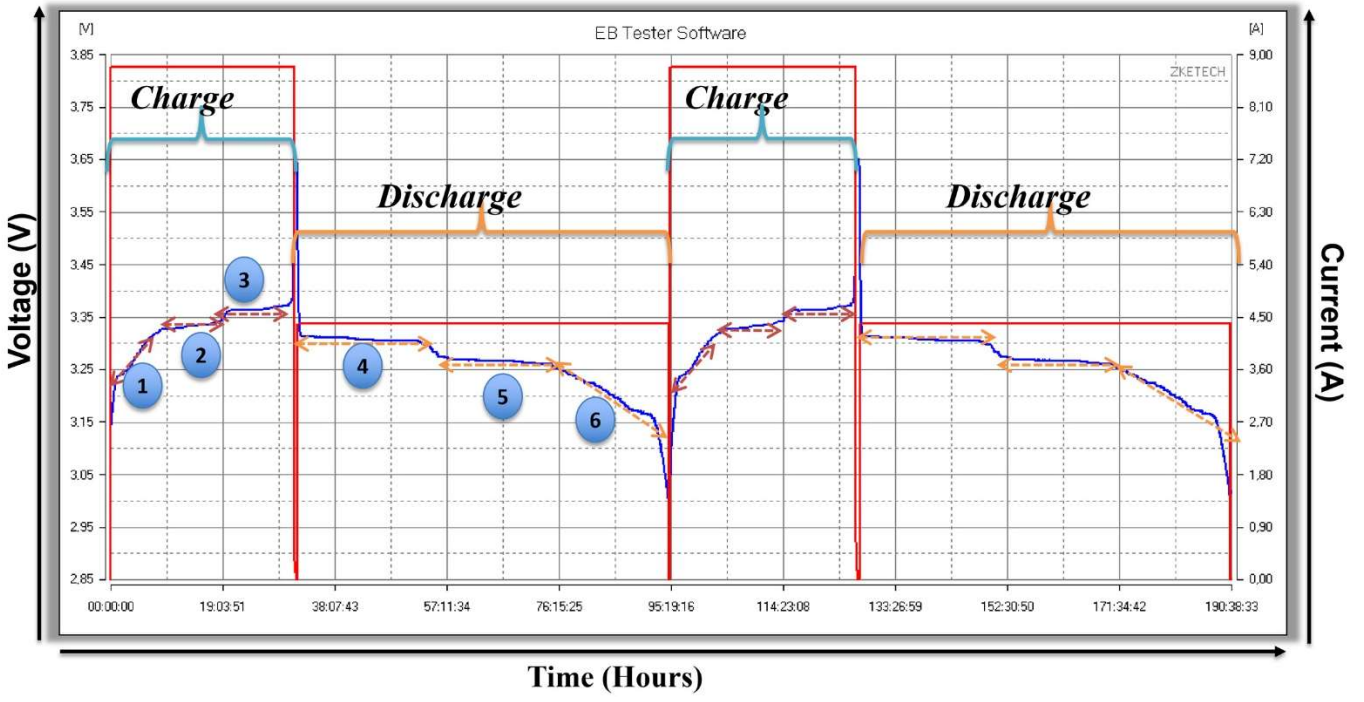

Figure 3. S-cell operating cycle under the slow scenario. The numbers indicate the following phases: (1) raw charge phase, (2) first intercalation phase, (3) second intercalation phase, (4) first deintercalation phase, (5) second deintercalation phase, (6) residual discharge phase.

The cycle trajectory is similar for both R and S cells, which are subjected, respectively, to high current (35.76 A/17.87 A) and low current (8.79 A/4.39 A) charge/discharge processes. This is evident from three phases (Figure 2 and 3), with the first phase during charging and the final phase during discharging having steep gradients. In contrast, two plateaus (numbers 2 and 3) occur in the charging section, and two plateaus (numbers 4 and 5) in the discharging section. For the R cells, the plateau or intercalation phases during charging represent nearly 60% of the total capacity, with a constant voltage around 3.4 V. Similarly, the two plateaus during discharging release almost 70% of the total stored energy while maintaining a constant voltage around 3.3 V. This performance is consistent with findings reported by Hu et al. (2011) [38] and Lin et al. (2022) [43], who also reported high efficiency and stability in $LiFePO_4$ batteries during charge and discharge cycles.

Effectiveness of Coulombic Efficiency as a Degradation Indicator

The change in Coulombic Efficiency (*CE*) values across all $LiFePO_4$ cells over five months (May–September 2022) is illustrated in Figure 4. The solid curves depict R-cells subjected to high current, while the dotted curves show chronological variations in S-cells under low current. R-cells underwent 146 cycles of 24-h charge and discharge periods, whereas S-cells underwent 35 cycles of 96-h charge/discharge periods. Despite both types of cells coming from the same supplier, the observed discrepancy between the two solid line curves of the R-cells indicates differences in their capacities. Despite these differences, the results indicate that neither R nor S cells showed a clear declining trend in coulombic efficiency (*CE*) from their initial value close to 1, and therefore failed to reveal ongoing degradation. *CE* for R-cells oscillated between 0.9967 and 1.0011, whereas for S-cells, values ranged from 0.9982 to 1.0000. This finding appears paradoxical since *CE* typically decreases over time from 1, rather than increasing.

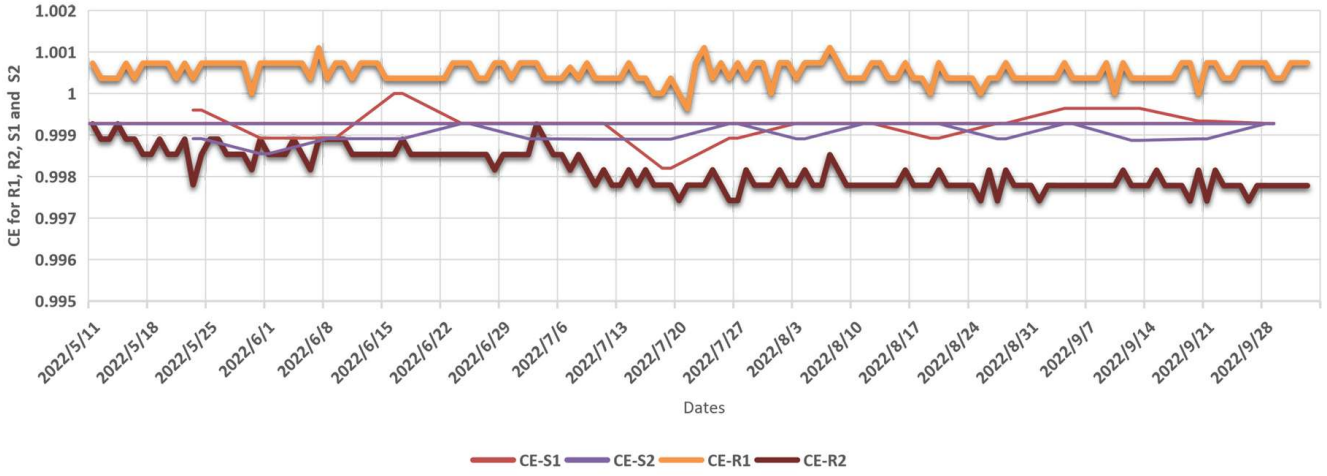

Figure 4. Variation in Coulombic Efficiency (*CE*).

Similar observations were reported by Dong et al. (2021) [44], who also observed inconsistent *CE* fluctuations. Although their measurement devices differ from the four A40L testers used in this study, it is unlikely that all four independent devices would have identical issues, as suggested by the graph patterns. Therefore, the Coulombic Efficiency (*CE*) indicator appears inadequate for tracking battery degradation under the tested field conditions.

Monitoring Cell Degradation Using Q_{cycle}

The change in Q_{cycle} values (total charged energy plus total discharged energy) for $LiFePO_4$ lithium-ion battery cells is shown in Figure 5. R-cells subjected to high currents are shown as lines, while S-cells subjected to low currents are represented by points. The clear and progressive decrease in Q_{cycle} is evident in Figure 5. Over a five-month period, comprising 146 cycles of 24 h for R-cells and 35 cycles of 96 h for S-cells, Q_{cycle} decreased by 7.8 Ah for R1, 7.0 Ah for R2, 3.9 Ah for S1, and 4.3 Ah for S2. This degradation is more pronounced in cells subjected to higher currents and a greater number of cycles. The exponential nature of the decline across all four curves indicates a consistent loss of individual cell capacities. This contrasts with the Coulombic Efficiency (*CE*) graphs, which showed no clear capacity decline during the testing period. Table 4 presents the capacity losses of the studied $LiFePO_4$ cells. On average, the energy available per cycle decreased by 6.25 ± 1.84 Ah over 5 months for all four cells, reflecting their reduced capacities.

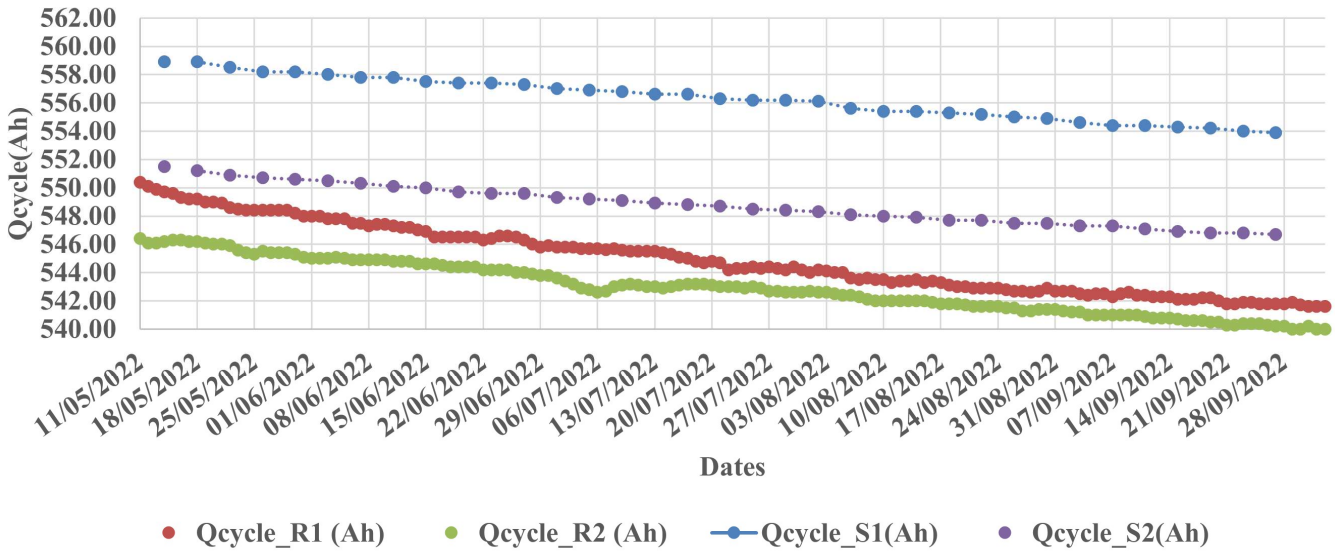

Figure 5. Variation in Q_{cycle} cell capacity.

Table 4. Variation of cell capacities over a five-month period.

$LiFePO_4$ cells	Capacity at beginning of tests (Ah)	Capacity at end of tests (Ah)	Variation (Ah)	Percentage variation (%)
R1	278.5	270.7	7.8	3%
R2	276.7	269.7	7	3%
S1	280.8	276.9	3.9	1%
S2	277.5	273.2	4.3	2%

Relationships among Time, Cell Capacity, Temperature, and Humidity

Under the experimental conditions, ambient temperatures and relative humidity within the open-air laboratory varied from 40 °C and 19% during the dry season (May) to 26.8 °C and 77.9% in September near the end of the rainy season. Figure 6 shows significant variations in temperature and relative humidity occurred between June 6 and June 9. Specifically, the maximum temperature dropped from nearly 40 °C on June 6 to 31 °C on June 8, while the maximum relative humidity increased from 37% on June 6 to 69% on June 9. These abrupt changes were attributable to the onset and establishment of the rainy season, which typically begins in late May and ends in late September or early October [45,46].

Q_{cycle} capacity decreased in parallel with the temperature, while relative humidity increased during this decline in Q_{cycle}. Although this phenomenon suggests a possible correlation, it does not establish causality between temperature decrease or relative humidity increase and the degradation of $LiFePO_4$ lithium-ion cells. Notably, as illustrated in Figures 6A–D, the observed variations in temperature and relative humidity did not noticeably disrupt the degradation process as measured by Q_{cycle} capacity of the $LiFePO_4$ battery cells, whether they were subjected to high current (R-cells) or low current (S-cells) operating conditions.

Pearson correlation coefficient values are presented after the summary statistics in Tables 5 and 6. The temperature was strongly and positively correlated with cycle capacity Q_{cycle}, while relative humidity was strongly and negatively correlated. The correlation coefficients for maximum temperature were 0.82 for R1, 0.78 for R2 (Table 5), 0.78 for S1, and 0.81 for S2 (Table 6). Similarly, relative humidity was strongly and negatively correlated with cycle capacity Q_{cycle}. The correlation coefficients for maximum relative humidity were −0.79 for R1, −0.76 for R2 (Table 5), −0.75 for S1, and −0.79 for S2 (Table 6). The same relationships were observed with the minimum values of temperature and relative humidity.

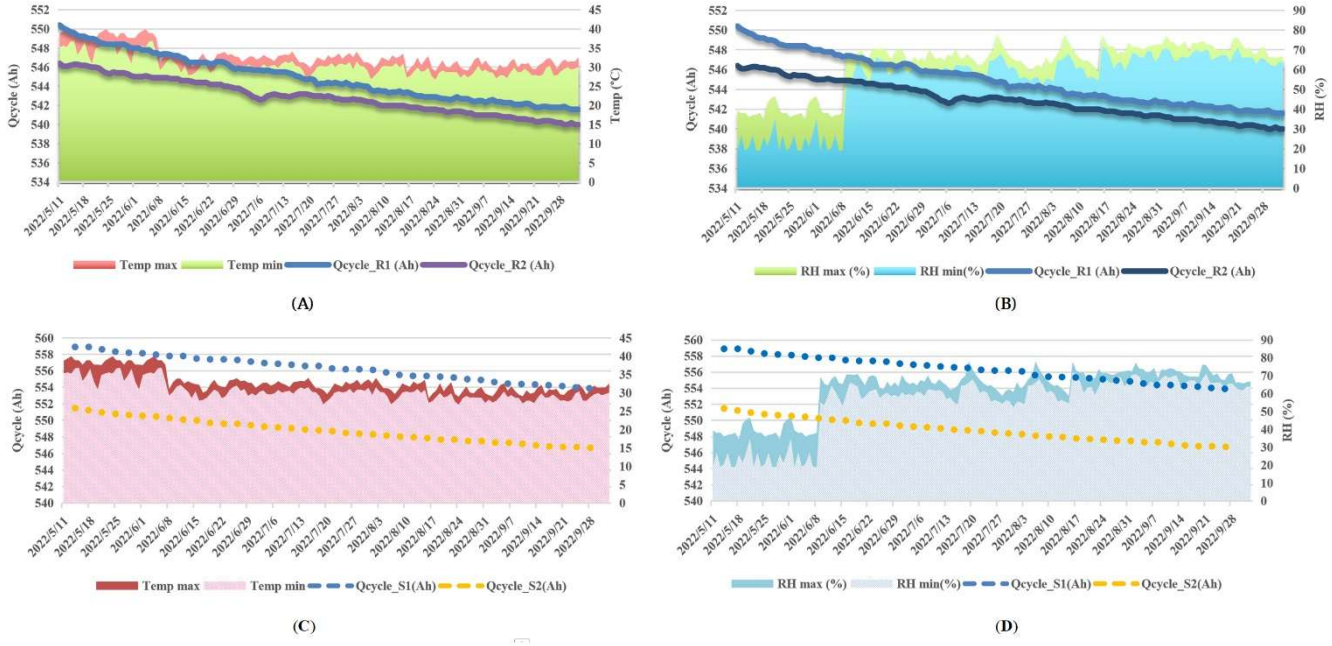

Figure 6. Temporal co-evolution of temperature (**A**,**C**), relative humidity (**B**,**D**), and Q_{cycle} capacity of $LiFePO_4$ cells under high current (R-cells) and low current (S-cells) conditions.

The relationships among the six operational and environmental variables (time *t*, Q_{cycle}, *Temp Max*, *Temp Min*, *RH Max*, and *RH Min*) are summarized in Figures 7 and 8 using Principal Component Analysis (PCA). The first two components, F1 and F2, captured the dominant variance patterns in battery behavior, accounting for 96.85% of the total variability in R1 and R2 cells and 88.17% in S1 and S2 cells. This high explanatory power confirms the consistency of the observed patterns across both battery groups. Notably, F1 alone accounted for 87.07% (R-cells) and 88.17% (S-cells) of the total variance, which made it the primary component of interest.

The first principal component (F1) was positively correlated with both Q_{cycle} and temperature (*Temp Max* and *Temp Min*), while time *t* and relative humidity (*RH Max* and *RH Min*) had negative loadings. This distribution showed that, within the observed range of 26.8 °C to 40.0 °C, Q_{cycle} was positively associated with temperature, while time and relative humidity were negatively associated with Q_{cycle} over the experimental period. These statistical associations are consistent with previous reports describing improved electrochemical kinetics at moderate temperatures and the potential influence of humid environments on battery aging [47–49]. However, because time, temperature and humidity varied together naturally during the seasonal transition covered by this study, PCA alone did not establish independent causal relationships between these environmental variables and battery degradation.

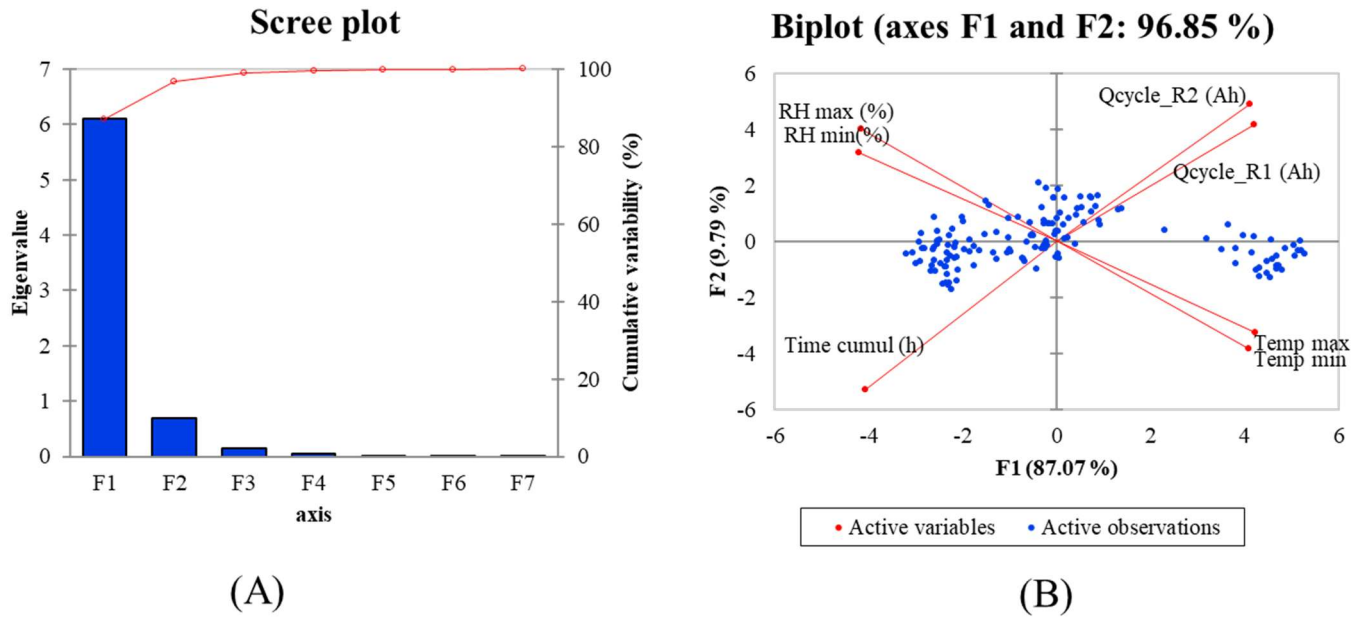

Figure 7. PCA results for R-cells. (**A**) Principal axes. (**B**) Variable loadings.

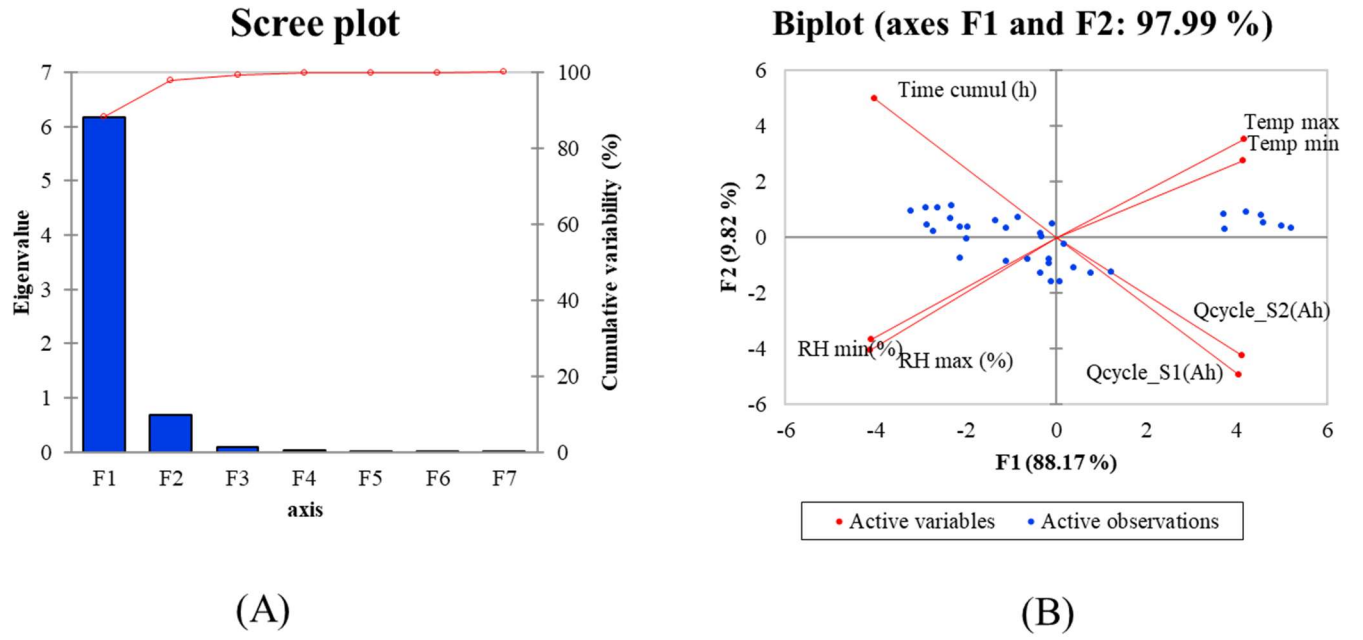

Figure 8. PCA results for S-cells. (**A**) Principal axes. (**B**) Variable loadings.

Table 5. Cells R1, R2, temperature *and RH* data summary and correlation matrix.

Summary statistics (Quantitative data):							
Variable	**Observations**	**Obs. with missing data**	**Obs. without missing data**	**Minimum**	**Maximum**	**Mean**	**Std. deviation**
Cumulative time (h)	146	0	146	24.0	3504.0	1764.0	1015.0
Q_{cycle}_R1 (Ah)	146	0	146	541.6	550.4	545.0	2.4
Q_{cycle}_R2 (Ah)	146	0	146	540.0	546.4	542.9	1.8
RH max (%)	146	0	146	34.4	77.9	62.7	12.5
RH min (%)	146	0	146	19.0	72.0	54.7	16.5
Temp max	146	0	146	28.5	40.0	33.1	3.0
Temp min	146	0	146	26.8	36.9	30.5	2.6
Correlation matrix (Pearson (n)):							
Variables	**Time cumul (h)**	**Q_{cycle}_R1 (Ah)**	**Q_{cycle}_R2 (Ah)**	***RH* max (%)**	***RH min (%)***	***Temp* max (°C)**	***Temp* min (°C)**
Time cumul (h)	1	−0.987	−0.992	0.734	0.765	−0.770	−0.728
Q_{cycle}_R1 (Ah)	−0.987	1	0.987	−0.789	−0.815	0.821	0.778
Q_{cycle}_R2 (Ah)	−0.992	0.987	1	−0.757	−0.789	0.786	0.741
RH max (%)	0.734	−0.789	−0.757	1	0.978	−0.935	−0.915
RH min (%)	0.765	−0.815	−0.789	0.978	1	−0.935	−0.877
Temp max (°C)	−0.770	0.821	0.786	−0.935	−0.935	1	0.949
Temp min (°C)	−0.728	0.778	0.741	−0.915	−0.877	0.949	1

Note: Red shaded areas denote strong negative correlation, while green areas show strong positive correlation.

Table 6. Cells S1, S2, *temperature and RH data* summary and correlation matrix.

Summary statistics (Quantitative data):							
Variable	**Observations**	**Obs. with missing data**	**Obs. without missing data**	**Minimum**	**Maximum**	**Mean**	**Std. deviation**
Time cumul (h)	35	0	35	96.0	3360.0	1728.0	983.7
Q_{cycle}_*S1 (Ah)*	35	0	35	553.9	558.9	556.3	1.5
Q_{cycle}_*S2 (Ah)*	35	0	35	546.7	551.5	548.8	1.4
RH max (%)	35	0	35	34.4	77.9	62.5	13.1
RH min (%)	35	0	35	19.0	69.5	54.3	16.5
Temp max	35	0	35	29.6	39.4	33.3	2.9
Temp min	35	0	35	26.9	36.9	30.7	2.7

Correlation matrix (Pearson (n)):							
Variables	**Time cumul (h)**	**Q_{cycle}_*S1 (Ah)***	**Q_{cycle}_*S2 (Ah)***	***RH* max (%)**	***RH* min (%)**	***Temp* max (°C)**	***Temp* min (°C)**
Time cumul (h)	1	−0.998	−0.995	0.751	0.763	−0.777	−0.790
Q_{cycle}_*S1 (Ah)*	−0.998	1	0.994	−0.754	−0.761	0.778	0.796
Q_{cycle}_*S2 (Ah)*	−0.995	0.994	1	−0.788	−0.799	0.811	0.822
RH max (%)	0.751	−0.754	−0.788	1	0.977	−0.966	−0.947
RH min (%)	0.763	−0.761	−0.799	0.977	1	−0.962	−0.906
Temp max (°C)	−0.777	0.778	0.811	−0.966	−0.962	1	0.962
Temp min (°C)	−0.790	0.796	0.822	−0.947	−0.906	0.962	1

Note: Red shaded areas denote strong negative correlation, while green areas show strong positive correlation.

Nonlinear Regression for Capacity Degradation

The results of applying the exponential decay model to the Q_{cycle} capacity data over time for the R-cells show a good curve fit to the data for both R cells, with symmetrically distributed residuals around zero for both the 116 observations used to calibrate the model and the 30 randomly selected observations for model validation. The equations for the R-cells are displayed in Table 7, with respective determination coefficients (R^2) of 0.97 for R1 and 0.98 for R2, and *MSE* and *RMSE* values very close to zero. This confirms the suitability of the exponential decay model in capturing variation in Q_{cycle} over time.

Table 7. Cell regression equations and lifespans.

Cell ID	Nonlinear regression equation	Goodness-of-fit statistics
Rapid charge/discharge R1	$Q_{cycle_{R1}}(t) = 549.1717 \cdot e^{-4.3559 \cdot 10^{-6} t}$	R^2 = 0.974 *MSE* = 0.163 *RMSE* = 0.403
Rapid charge/discharge R2	$Q_{cycle_{R2}}(t) = 546.10523 \cdot e^{-3.2931 \cdot 10^{-6} t}$	R^2 = 0.982 *MSE* = 0.057 *RMSE* = 0.239
Slow charge/discharge S1	$Q_{cycle_{S1}}(t) = 558.9913 \cdot e^{-2.7749 \cdot 10^{-6} t}$	R^2 = 0.996 *MSE* = 0.010 *RMSE* = 0.100
Slow charge/discharge S2	$Q_{cycle_{S2}}(t) = 551.2380 \cdot e^{-2.5789 \cdot 10^{-6} t}$	R^2 = 0.990 *MSE* = 0.022 *RMSE* = 0.150

The results of applying the exponential decay model to the Q_{cycle} capacity data over time for the S-cells show an excellent curve fit to the data for both S-cells, as shown by symmetrically distributed residuals around zero for both the 25 observations used for model calibration and the 10 randomly selected observations for validation. Equations for the S-cells are presented in Table 7, with determination coefficients (R^2) of 0.99 for both S1 and S2, alongside *MSE* and *RMSE* values closer to zero than the R-cells.

Estimation of Battery Lifespan

The use of Microsoft Excel's Goal Seek tool with the equations presented in Table 7 enabled the estimation of the lifespans of the four $LiFePO_4$ cells, with results presented in Table 8. The cells subjected to high currents and undergoing 146 cycles of charge/discharge, i.e., the R-cells, had theoretical lifespans of 24.0 years and 31.7 years, respectively. For cells subjected to lower currents, i.e., the S-cells, the theoretical lifespan projections were 37.7 and 40.6 years, respectively. These results are clustered near 40 years.

Table 8. Expected cell lifespans.

Cell ID	Initial capacity Q_{cycle0} (Ah)*	$Q_{cyclemin}$ = 40% × Q_{cycle0} (Ah)	Expected lifespan (years)
Rapid charge/discharge R1	549.17	219.67	24.0
Rapid charge/discharge R2	546.10	218.44	31.7
Slow charge/discharge S1	558.99	223.60	37.7
Slow charge/discharge S2	551.24	220.49	40.6

*Note: Initial cycle capacities (Q_{cycle0}) represent the y-intercept of the fitted exponential decay model at t = 0 rather than the arithmetic sum of the manufacturer-rated nominal capacity (Table 1). The slight offset reflects actual initial conditions, including coulombic losses and cell-to-cell manufacturing variability.

DISCUSSION

Interpretation of Charge/Discharge Cycle Characteristics

The stability of the voltage plateaus observed in both R and S cells is an important advantage of $LiFePO_4$ batteries, as many devices used in installations, such as refrigerators and microwaves in domestic settings, and pumps and mills in rural settings, require a consistent operating voltage. The final phase of the discharge trajectory (number 6) releases the remaining 30% of the energy over a relatively short period of 4 h (for high current) or 6 h (for low current), resulting in a steep gradient. This behavior was consistent with the results obtained by Khairunnisa et al. (2023) [40], who reported similar rapid energy release characteristics in the final discharge phase of their $LiFePO_4$ battery studies. These observations highlight the consistency and reliability of $LiFePO_4$ batteries in maintaining stable voltage outputs, thereby supporting the proper functioning of various electronic devices and machinery.

Analysis of Degradation Indicators: *CE* vs. Q_{cycle}

The inadequacy of Coulombic Efficiency (*CE*) as a reliable degradation indicator in semi-field conditions is an important result of this study. The high sensitivity of *CE* to small measurement errors, arising from its mathematical formulation as a ratio (Q_D/Q_C), makes it unsuitable for field deployments where instrumentation precision is inherently limited. This conclusion is consistent with findings from Dong et al. (2021) [44], who questioned the reliability of *CE* as a sole indicator of battery health. In contrast, Q_{cycle} is a more suitable metric for showing capacity degradation of $LiFePO_4$ cells over time, offering reduced error propagation and greater stability across measurement fluctuations.

Comparison with other published findings supports these observations regarding the degradation behavior of lithium-ion battery cells under cycling conditions. Madej and Wojciechowski (2021) [36] similarly report exponential declines in capacity metrics over extended cycling periods, noting variations in degradation rates influenced by cell design, electrode materials, and operational parameters. These studies are consistent with our findings, indicating the general nature of capacity loss in $LiFePO_4$ cells under varied experimental conditions. Moreover, recent research by Zhou et al. (2023) [42] provides evidence on the mechanisms underlying

capacity degradation, attributing it to irreversible structural changes and material degradation over cycling. This body of literature supports the reliability of Q_{cycle} as a metric for evaluating long-term battery performance across different experimental settings.

Environmental Factors and Battery Degradation

Earlier work by Kurpiel et al. (2021) [50] and Martin et al. (2008) [51] showed that lithium-ion cells tolerate ordinary temperature and humidity shifts without abrupt capacity loss. This holds true, however, only when the environment remains within moderate bounds. In rural pumping stations (A practical demonstration of the solar pumping system and its operation with lithium batteries is provided in the supplementary videos (Videos S1–S4)), poor ventilation, with doors and windows kept shut, traps heat and moisture, producing sharp indoor spikes that accelerate wear. Conversely, keeping openings unobstructed allows air to move freely, smoothing out daily and seasonal swings. Under such naturally ventilated conditions, the steady fade tracked by Q_{cycle} offers a reliable basis for maintenance planning, without requiring costly climate control.

The second component, F2, accounted for an additional 9.79% of variability for R1 and R2 and 9.82% for S1 and S2, and was primarily influenced by time t and Q_{cycle} in opposite directions. A strong negative loading of time t on F1 and F2 indicates that battery degradation is time-dependent, reinforcing the effectiveness of Q_{cycle} as a metric for tracking capacity loss. The observed statistical associations between Q_{cycle}, temperature, and humidity [52] further show the importance of monitoring environmental conditions during battery operation. However, because these environmental variables evolved simultaneously with cycling time throughout the experiment, their individual contributions to battery degradation could not be isolated from the present dataset. Consequently, the PCA should be viewed as identifying correlations among operational and environmental variables rather than demonstrating independent causal mechanisms.

These results support the choice of Q_{cycle} as a key performance indicator, showing its ability to capture degradation trends more effectively than Coulombic Efficiency (CE), particularly in environments with moderate temperature fluctuations and variable humidity levels.

Throughout the experiments, the cells were charged with a $LiFePO_4$-compatible algorithm. However, inadequate charging protocols, characterized by mismatched voltage targeting, absence of current tapering, and unsupervised float stages, can accelerate degradation through parasitic reactions and loss of lithium inventory [53]. These effects were not examined here; instead, the setup excluded such mismatches so that ambient factors could be observed in isolation. The Q_{cycle} patterns therefore reflect battery behavior under sound charge management yet naturally variable surroundings, showing that real-

world performance depends on both algorithm compatibility and local climate.

Mechanisms of Battery Degradation

Battery degradation in $LiFePO_4$ cells results primarily from the growth of the solid electrolyte interphase (SEI) layer at the anode-electrolyte boundary [54]. This passivation film forms during initial charging as the electrolyte decomposes and reacts with lithium ions and graphite. Once established, it supports stable cycling by shielding the electrolyte from direct electron contact. Yet continued thickening immobilizes lithium irreversibly, raises internal resistance, and progressively reduces available capacity [24,43,55]. Electrolyte gelification worsens this effect by further limiting ion transport [43].

The process resembles radioactive decay: just as fewer nuclei undergo emission over time, fewer lithium ions remain electrochemically active as the SEI layer expands, gradually reducing the energy the cell can deliver [24,55,56].

In the context of batteries, passivation refers to the formation of an insulating layer on the electrodes, which limits the effective participation of lithium ions in the electrochemical reactions needed for energy release. This phenomenon limits the battery's ability to maintain its original energy output over its operational life. Thus, although $LiFePO_4$ batteries are known for their durability and stability, their performance diminishes as the passivation layer grows, similar to decreasing emission from radioactive nuclei [24].

Factors That Can Shorten Battery Lifespan

Extreme Temperatures

Environmental conditions during operation play an important role, with temperature being particularly significant. Research has shown that deviations from the optimal temperature range can significantly affect battery performance and longevity [48]. For example, studies indicate that $LiFePO_4$ batteries typically perform best within a temperature range of −10 to 60 °C, beyond which their capacity can deteriorate rapidly [48]. Moreover, mechanical stresses such as vibrations and shocks can accelerate battery degradation and increase the risk of functional failures [48]. Additionally, external mechanical events such as crashes can pose safety risks and further shorten battery life.

Chemical Environment and Manufacturing Conditions

The chemical environment around the battery also contributes to its degradation. Factors such as ambient humidity can expose cells to moisture, which may corrode internal components and reduce battery efficiency over time [57]. Finally, the quality of the $LiFePO_4$ battery itself is a key determinant of its lifespan. Variations in manufacturing processes,

materials used, and quality control standards can cause substantial differences in battery performance and durability. High-quality batteries often use higher-quality electrode materials and advanced battery management systems, enhancing safety and extending lifespan [58]. Investing in high-quality $LiFePO_4$ batteries from reputable manufacturers may initially cost more but can ultimately result in more reliable performance and longer lifespan, making them a suitable choice for critical applications [49].

Implications for Sustainable Solar Irrigation

The projected lifespans of 32–41 years for three of the four cells (mean 37 ± 5 years) challenge the prevailing view that batteries are the weak link in solar irrigation economics. The R1 outlier at 24 years, detectable only through Q_{cycle}*'s* cell-level resolution, supports the metric's sensitivity and cautions against universal lifespan prediction without individual calibration. If these projections are confirmed under broader validation, $LiFePO_4$ storage could outlast pumps, pipes, and even PV panels, shifting the financial calculus for rural investors from frequent replacement cycles toward long-term asset management. This interpretation matters for development finance: it could lower the perceived risk of off-grid energy projects and strengthen the case for capital expenditure over operational subsidies in rural Africa.

The next technical steps include pack-scale validation of Q_{cycle} under real farm loads, integration with smart charge controllers, and coupling to machine-learning diagnostics that can detect degradation before it compromises irrigation schedules.

Study Limitations and Scope Boundaries

Several methodological limitations shape the interpretation of the present findings. First, the experimental window covered five months (May–September 2022), capturing one complete seasonal cycle but not the multi-year trajectory. Degradation-regime transitions("knees") have been reported in many Li-ion aging studies but are not systematically observed under all chemistries, operating conditions, or time scales [59,60]. Several studies have shown that early-stage degradation often follows smooth monotonic behavior before possible transitions to accelerated aging later in life [16,53,61]. Consequently, the exponential model proposed here should be interpreted as describing the observed degradation regime during the experimental window. Extrapolation beyond this window depends on the absence of subsequent degradation regime transitions and therefore represents a theoretical projection and requires long-term validation.

Second, the sample included only four cells of identical rated capacity (280 Ah) sourced from a single manufacturing batch. Although this sample size was sufficient to evaluate the consistency of the proposed Q_{cycle} metric under controlled experimental conditions, it was not intended to provide statistically representative lifetime estimates for the broader population of commercial $LiFePO_4$ cells. The convergence (Table 8) of R2, S1, and S2 on a 31.7–40.6-year projection (mean 36.7 ± 4.5 years) suggests that Q_{cycle} captured a reproducible degradation signature under comparable operational conditions. The downward deviation of R1 to 24.0 years, despite sharing the identical cycling protocol and batch origin with R2, likely reflects latent cell-to-cell manufacturing heterogeneity rather than methodological instability. Q_{cycle}'s resolution of this individual variation, which Coulombic Efficiency cannot resolve, highlights its diagnostic value for cell-specific tracking. It also cautions against applying a single decay rate to untested cells without prior calibration. The results therefore represent cell-level behavior under the specific electrochemical parameters investigated. Consequently, the reported lifespan projections should be interpreted as cell-specific model outputs rather than population-level estimates. Generalizing these results to other $LiFePO_4$ cells, production batches, chemistries, or form factors requires validation with substantially larger datasets. Since the sample size per group was only two cells, statistically meaningful confidence intervals for population-level lifespan predictions could not be reliably estimated. Therefore, the data in this study are primarily used to qualitatively validate the degradation trend captured by Q_{cycle} rather than to quantitatively calibrate absolute lifespan.

Third, tests were conducted under semi-field conditions using programmable DC testers rather than actual solar-pump loads. While this approach isolated environmental and electrical variables, it did not capture transient phenomena inherent to real photovoltaic irrigation systems, such as partial state-of-charge operation, intermittent shading, or pump-start inrush currents, which may accelerate degradation beyond the trends reported here.

Fourth, the correlation structure revealed by PCA indicates a statistical association rather than demonstrated causation. Temperature and humidity co-vary seasonally with Q_{cycle}, yet the underlying electrochemical mechanisms (SEI thickening, electrolyte gelification, terminal corrosion) were not verified by post-mortem analysis (e.g., electrochemical impedance spectroscopy, SEM imaging, or electrolyte assay). Moreover, because the experiment covered a single seasonal transition from the dry to the rainy season, cycling time, temperature, and relative humidity evolved simultaneously throughout the monitoring period. Consequently, the present dataset does not allow independent contributions of these variables to battery degradation to be separated statistically. Future work should combine Q_{cycle} tracking with destructive diagnostics to address this mechanistic gap.

Finally, the lifespan projection assumes that cells are operated within the voltage and current envelopes defined in this study. Deviations, such as mismatched charging algorithms (e.g., lead-acid profiles), sustained over-temperature events above 45 °C, or deep discharges below 3.0 V, could invalidate the exponential trajectory and substantially shorten operational life.

CONCLUSIONS

This study introduces and validates Q_{cycle} as a field-robust metric for tracking $LiFePO_4$ degradation in Sahelian solar irrigation contexts. Whereas Coulombic Efficiency produced erratic signals under natural temperature and humidity swings, Q_{cycle} yielded a steady, monotonically declining trace across both rapid and slow cycling regimes during the five-month semi-field campaign. Nonlinear regression modeled this decay accurately ($R^2 > 0.97$), producing a theoretical projection of cell longevity under the assumption of sustained exponential degradation.

These results have immediate practical relevance for the water–energy–food nexus. Q_{cycle} offers technicians and farmers a straightforward diagnostic tool that requires no laboratory-grade instrumentation, bridging electrochemical research and the management of decentralized systems. Additionally, the methodology sets a reproducible baseline for comparing battery stress across contrasting climatic seasons, which is necessary for predictive maintenance frameworks in the Sahel.

The results also highlight the importance of cell-level monitoring when assessing battery degradation. The observed differences among cells indicate that a single degradation trajectory should not be universally applied without appropriate validation and calibration. The absence of a "knee" during the present five-month observation period should not be interpreted as evidence that none will occur later. Instead, the exponential model should be viewed as describing the degradation regime observed during the experimental window, while future multi-year monitoring should determine whether regime transitions eventually develop. Future studies involving larger samples from multiple production batches are also required to assess the generalizability of the observed degradation trends and to evaluate whether subsequent degradation regime transitions may occur. Future work should further investigate the implementation of Q_{cycle} within Battery Management Systems (BMS), where cumulative partial charge and discharge events can be combined into Equivalent Full Cycles for continuous degradation monitoring under real operating conditions.

By basing battery health assessment on locally measurable metrics rather than laboratory abstractions, this work advances SDG 7 targets for resilient, affordable clean energy and contributes to climate-resilient agricultural change across semi-arid regions of the Global South.

SUPPLEMENTARY MATERIALS

The following supplemental materials are available online, Video S1: Modern solar pumping with lithium batteries [FRENCH] Part 1: https://www.youtube.com/watch?v=KDfUnk3faD0, Video S2: Modern solar pumping with lithium batteries [FRENCH] Part 2: https://www.youtube.com/watch?v=sbiMgXFhGJE&t=164s, Video S3: Modern solar pumping with lithium batteries [FRENCH] Part 3: https://www.youtube.com/watch?v=Vzaz31sJ2mU, Video S4: Modern solar pumping with lithium batteries [FRENCH] Part 4: https://www.youtube.com/watch?v=FKsXBo9Z3vY.

DATA AVAILABILITY

The study dataset is available from the authors upon reasonable request.

AUTHOR CONTRIBUTIONS

Conceptualization, AK; methodology, AK and SK; investigation, AK and SK; validation and formal analysis, DY; simulation and visualization, SK and DDD; writing: original draft preparation, AK, DY and SK; writing: review and editing, DDD; supervision, AK and DY. All authors have read and agreed to the published version of the manuscript.

CONFLICTS OF INTEREST

The authors report no relevant financial or non-financial interests.

FUNDING

This work was financially supported by the World Bank through its Africa Higher Education Centres of Excellence (ACE) (Grant number IDA 6388-BF/D443-BF), of which the International Institute for Water and Environmental Engineering (2iE) is a partner. However, the World Bank was not involved in the study design, data collection, data analysis and interpretation, writing of the report, or the decision to submit the article for publication.

ACKNOWLEDGMENTS

The authors thank the World Bank Group and the Government of Burkina Faso for financial support through the Africa Higher Education Centers of Excellence for Development Impact project.

REFERENCES

1. Reiter MA, Barresi PA. Meeting our sustainability challenges. J Sustain Res. 2019;1(1): e190001. doi: 10.20900/jsr20190001

2. Henderson B, Lankoski J. Evaluating the environmental impact of agricultural policies. OECD Food, Agriculture and Fisheries Papers. Paris (France): OECD Publishing; 2019. Report No.: 130. doi: 10.1787/add0f27c-en
3. IFAD. Transformation de l'agriculture en Afrique de l'Ouest–défis et opportunités (2030-2050-2063) [Transformation of agriculture in West Africa: challenges and opportunities (2030-2050-2063)]. Inter-réseaux. Available from: https://www.inter-reseaux.org/ressource/transformation-de-lagriculture-en-afrique-de-louest-defis-et-opportunites-2030-2050-2063/. Accessed on 2026 May 19.
4. Hajikhani A, Suominen A. Mapping the sustainable development goals (SDGs) in science, technology and innovation: application of machine learning in SDG-oriented artefact detection. Scientometrics. 2022;127:6661-93. doi: 10.1007/s11192-022-04358-x
5. Meschede C. The sustainable development goals in scientific literature: a bibliometric overview at the meta-level. Sustainability. 2020;12(11):4461. doi: 10.3390/su12114461
6. Tzone Digital Technology Co., Ltd, R&D Team. TempU08B data logger software. Shenzhen (China): Tzone Digital Technology Co., Ltd; 2026. Available from: https://d.tzonedigital.com/. Accessed on 2026 May 18.
7. Sarasketa-Zabala E, Gandiaga I, Rodriguez-Martinez LM, Villarreal I. Calendar aging analysis of a $LiFePO_4$/graphite cell with dynamic model validations: towards realistic lifetime predictions. J Power Sources. 2014;272:45-57. doi: 10.1016/j.jpowsour.2014.08.051
8. Kanteh Sakiliba S, Sani Hassan A, Wu J, Saja Sanneh E, Ademi S. Assessment of stand-alone residential solar photovoltaic application in sub-Saharan Africa: a case study of Gambia. J Renew Energy. 2015:640327. doi: 10.1155/2015/640327
9. Kothe S, Pfeifroth U, Cremer R, Trentmann J, Hollmann R. A satellite-based sunshine duration climate data record for Europe and Africa. Remote Sens. 2017;9(5):429. doi: 10.3390/rs9050429
10. Pereira LS, Allen RG, Smith M, Raes D. Crop evapotranspiration estimation with FAO56: past and future. Agric Water Manag. 2015;147:4-20. doi: 10.1016/j.agwat.2014.07.031
11. Inter-Réseaux. Promotion de la technologie de micro-aspersion: l'expérience du projet PRECIS dans le Centre-Est du Burkina Faso [Promotion of micro-sprinkler technology: the experience of the PRECIS project in the Centre-East of Burkina Faso]. Available from: https://www.inter-reseaux.org/ressource/promotion-de-la-technologie-de-micro-aspersion-lexperience-du-projet-precis-dans-le-centre-est-du-burkina-faso/. Accessed on 2024 June 21.
12. SONABEL. Branchements [Electrical connections]. Available from: https://eguichet.sonabel.bf/. Accessed on 2024 June 21.
13. Madani SS, Schaltz E, Kær SK. Effect of current rate and prior cycling on the coulombic efficiency of a lithium-ion battery. Batteries. 2019;5(3):57. doi: 10.3390/batteries5030057

14. Schulze MC, Neale NR. Half-cell cumulative efficiency forecasts full-cell capacity retention in lithium-ion batteries. ACS Energy Lett. 2021;6(3):1082-6. doi: 10.1021/acsenergylett.1c00173
15. Barré A, Deguilhem B, Grolleau S, Gerdard M, Suard F, Riu D. A review on lithium-ion battery ageing mechanisms and estimations for automotive applications. J Power Sources. 2013;241:680-9. doi: 10.1016/j.jpowsour.2013.05.040
16. Schmalstieg J, Käbitz S, Ecker M, Sauer DU. A holistic aging model for Li(NiMnCo)O_2 based 18650 lithium-ion batteries. J Power Sources. 2014;257:325-34. doi: 10.1016/j.jpowsour.2014.02.012
17. Berecibar M, Garmendia M, Gandiaga I, Crego J, Villarreal I. State of health estimation algorithm of $LiFePO_4$ battery packs based on differential voltage curves for battery management system application. Energy. 2016;103:784-96. doi: 10.1016/j.energy.2016.02.163
18. Namdari A, Li Z. An entropy-based approach for modeling lithium-ion battery capacity fade. Proceedings of 2020 Annual Reliability and Maintainability Symposium (RAMS); 2020 Jan 27–30; Palm Springs, CA, USA. p. 1-7. doi: 10.1109/RAMS48030.2020.9153698
19. Goh T, Park M, Seo M, Kim JG, Kim SW. Capacity estimation algorithm with a second-order differential voltage curve for Li-ion batteries with NMC cathodes. Energy. 2017;135:257-68. doi: 10.1016/j.energy.2017.06.141
20. An SJ, Li J, Daniel C, Mohanty D, Nagpure S, Wood DL. The state of understanding of the lithium-ion-battery graphite solid electrolyte interphase (SEI) and its relationship to formation cycling. Carbon. 2016;105:52-76. doi: 10.1016/j.carbon.2016.04.008
21. Gao Z, Xie H, Yang X, Niu W, Li S, Chen S. The dilemma of C-rate and cycle life for lithium-ion batteries under low temperature fast charging. Batteries. 2022;8(11):234. doi: 10.3390/batteries8110234
22. Korsaga E, Koalaga Z, Bonkoungou D, Zougmoré F. Comparaison et détermination des dispositifs de stockage appropriés pour un système photovoltaïque autonome en zone sahélienne [Comparison and determination of appropriate storage devices for a stand-alone photovoltaic system in the Sahelian zone]. J Int Technol Innov Phys. 2018;4(1). doi: 10.18145/jitipee.v4i1.161
23. Pilali E, Shafiei S, Salimi M, Amidpour M, Soltani M. Techno-economic–environmental assessment of PV–second-life battery systems with PCM-assisted thermal management in low peak-load residential grids of Iran. Results Eng. 2026;29:109038. doi: 10.1016/j.rineng.2026.109038
24. Lyu D, Ren B, Li S. Failure modes and mechanisms for rechargeable lithium-based batteries: a state-of-the-art review. Acta Mech. 2019;230(3):701. doi: 10.1007/s00707-018-2327-8

25. Sawadogo W, Neya T, Semde I, Korahiré JA, Combasséré A, Traoré DE, et al. Potential impacts of climate change on the Sudan-Sahel region in West Africa–insights from Burkina Faso. Environ Chall. 2024;15:100860. doi: 10.1016/j.envc.2024.100860
26. Bouniol D, Guichard F, Barbier J, Couvreux F, Roehrig R. Sahelian heat wave characterization from observational data sets. J Geophys Res Atmos. 2021;126(11):e2020JD034465. doi: 10.1029/2020JD034465
27. Pohl B, Dos Santos S, Bai GM, Compaoré Y, Dianou K, Diallo-Dudek J, et al. Indoor temperature variability in the Sahel: a pilot study in Ouagadougou, Burkina Faso. Theor Appl Climatol. 2021;146(3):1403-20. doi: 10.1007/s00704-021-03800-z
28. Zhang X, Sun P, Wang S, Zhu Y. Experimental study of the degradation characteristics of $LiFePO_4$ and $LiNi_{0.5}Co_{0.2}Mn_{0.3}O_2$ batteries during overcharging at low temperatures. Energies. 2023;16(6):2786. doi: 10.3390/en16062786
29. Addinsoft. XLSTAT statistical software: version 2019.2.2. 2019. Available from: https://www.xlstat.com. Accessed on 2023 May 7.
30. Vidal NP, Manful CF, Pham TH, Stewart P, Keough D, Thomas R. The use of XLSTAT in conducting principal component analysis (PCA) when evaluating the relationships between sensory and quality attributes in grilled foods. MethodsX. 2020;7:100835. doi: 10.1016/j.mex.2020.100835
31. Bro R, Smilde AK. Principal component analysis. Anal Methods. 2014;6(9):2812-31. doi: 10.1039/C3AY41907J
32. Archontoulis SV, Miguez FE. Nonlinear regression models and applications in agricultural research. Agron J. 2015;107:786-98. doi: 10.2134/agronj2012.0506
33. Huang HH, He Q. Nonlinear regression analysis. In: Meloun M, Militky J, editors. Comprehensive chemometrics. 2nd ed. Amsterdam (Netherlands): Elsevier; 2022. doi: 10.1016/B978-0-12-818630-5.10068-5
34. Chai T, Draxler RR. Root mean square error (RMSE) or mean absolute error (MAE)?–Arguments against avoiding RMSE in the literature. Geosci Model Dev. 2014;7:1525-34. doi: 10.5194/gmd-7-1247-2014
35. Chicco D, Warrens MJ, Jurman G. The coefficient of determination R-squared is more informative than SMAPE, MAE, MAPE, MSE and RMSE in regression analysis evaluation. PeerJ Comput Sci. 2021;7:e623. doi: 10.7717/peerj-cs.623
36. Madej W, Wojciechowski A. Analysis of the charging and discharging process of $LiFePO_4$ battery pack. Energies. 2021;14(13):4055. doi: 10.3390/en14134055
37. Tseng YM, Huang HS, Chen LS, Tsai JT. Characteristic research on lithium iron phosphate battery of power type. MATEC Web Conf. 2018;185:00004. doi: 10.1051/matecconf/201818500004
38. Hu Y, Liu H, Zhang Y, Liu K. Charging method research for lithium iron phosphate battery. Procedia Eng. 2011;15:4367-71. doi: 10.1016/j.proeng.2011.08.820

39. Han X, Feng X, Ouyang M, Lu L, Li J, Zheng Y, et al. A comparative study of charging voltage curve analysis and state of health estimation of lithium-ion batteries in electric vehicles. Automot Innov. 2019;2:263-75. doi: 10.1007/s42154-019-00080-2
40. Khairunnisa K, Mafturoh S. Characteristics of $LiFePO_4$ and Li-ion batteries during the process of charging and discharging for recommendation solar power energy storage. J Edukasi Elektro. 2023;7:53-62. doi: 10.21831/jee.v7i1.61654
41. Schmitt J, Rehm M, Karger A, Jossen A. Capacity and degradation mode estimation for lithium-ion batteries based on partial charging curves at different current rates. J Energy Storage. 2023;59:106517. doi: 10.1016/j.est.2022.106517
42. Zhou X, Han X, Wang Y, Lu L, Ouyang M. A data-driven $LiFePO_4$ battery capacity estimation method based on cloud charging data from electric vehicles. Batteries. 2023;9(3):181. doi: 10.3390/batteries9030181
43. Lin Y, Zhang X, Liu Y, Wang Q, Lin C, Chen S, et al. Ultra-stable Li||$LiFePO_4$ batteries via advanced designing of localized high concentration electrolyte. J Colloid Interface Sci. 2022;628:14-23. doi: 10.1016/j.jcis.2022.08.018
44. Dong H, Huang W, Zhao Y. Low complexity state-of-charge estimation for lithium-ion battery pack considering cell inconsistency. J Power Sources. 2021;515:230599. doi: 10.1016/j.jpowsour.2021.230599
45. Nicholson SE. Climate of the Sahel and West Africa. In: Oxford research encyclopedia of climate science. Oxford (UK): Oxford University Press; 2018. doi: 10.1093/acrefore/9780190228620.013.510
46. Sylla M, Nikiema M, Gibba P, Kebe I, Klutse NAB. Climate change over West Africa: recent trends and future projections. In: Yaro JA, Hesselberg J, editors. Adaptation to climate change and variability in rural West Africa. Cham (Switzerland): Springer; 2016. p. 25-40. doi: 10.1007/978-3-319-31499-0_3
47. Leng F, Tan CM, Pecht M. Effect of temperature on the aging rate of Li ion battery operating above room temperature. Sci Rep. 2015;5:12967. doi: 10.1038/srep12967
48. Waldmann T, Wilka M, Kasper M, Fleischhammer M, Wohlfahrt-Mehrens M. Temperature dependent aging mechanisms in lithium-ion batteries–a post-mortem study. J Power Sources. 2014;262:129-35. doi: 10.1016/j.jpowsour.2014.03.112
49. Han X, Xia S, Cao J, Wang C, Chen MG. Effect of humidity on properties of lithium-ion batteries. Int J Electrochem Sci. 2021;16:210554. doi: 10.20964/2021.05.54
50. Kurpiel W, Polnik B, Orzech Ł, Lesiak K, Miedziński B, Habrych M, et al. Influence of operation conditions on temperature hazard of lithium-iron-phosphate ($LiFePO_4$) cells. Energies. 2021;14(20):6728. doi: 10.3390/en14206728
51. Martin J, Yamada A, Kobayashi G, Nishimura S, Kanno R, Guyomard D, et al. Air exposure effect on $LiFePO_4$. Electrochem Solid-State Lett. 2008;11:A12-6. doi: 10.1149/1.2801016

52. Liebig G, Kirstein U, Geißendörfer S, Zahid O, Schuldt F, Agert C. The impact of environmental factors on the thermal characteristic of a lithium–ion battery. Batteries. 2020;6(1):3. doi: 10.3390/batteries6010003
53. Birkl CR, Roberts MR, McTurk E, Bruce PG, Howey DA. Degradation diagnostics for lithium ion cells. J Power Sources. 2017;341:373-86. doi: 10.1016/j.jpowsour.2016.12.011
54. Shinagawa C, Ushiyama H, Yamashita K. Multiscale simulations for lithium-ion batteries: SEI film growth and capacity fading. J Electrochem Soc. 2017;164(13):A3018. doi: 10.1149/2.0381713jes
55. Kabir MM, Demirocak D. Degradation mechanisms in Li-ion batteries: a state-of-the-art review. Int J Energy Res. 2017;41. doi: 10.1002/er.3762
56. Kaneko G, Inoue S, Taniguchi K, Hirota T, Kamiya Y, Daisho Y, et al. Analysis of degradation mechanism of lithium iron phosphate battery. World Electr Veh J. 2013;6:555-61. doi: 10.3390/wevj6030555
57. Kosfeld M, Westphal B, Kwade A. Moisture behavior of lithium-ion battery components along the production process. J Energy Storage. 2023;57:106174. doi: 10.1016/j.est.2022.106174
58. Duan J, Tang X, Dai H, Yang Y, Wu W, Wei X, et al. Building safe lithium-ion batteries for electric vehicles: a review. Electrochem Energy Rev. 2020;3:1-42. doi: 10.1007/s41918-019-00060-4
59. Sui X, Świerczyński M, Teodorescu R, Stroe DI. The degradation behavior of $LiFePO_4$/C batteries during long-term calendar aging. Energies. 2021;14(6):1732. doi: 10.3390/en14061732
60. Attia PM, Bills A, Planella FB, Dechent P, Reis G dos, Dubarry M, et al. “Knees” in lithium-ion battery aging trajectories. J Electrochem Soc. 2022;169:060517. doi: 10.1149/1945-7111/ac6d13
61. Keil P, Schuster SF, Wilhelm J, Travi J, Hauser A, Karl RC, et al. Calendar aging of lithium-ion batteries: I. Impact of the graphite anode on capacity fade. J Electrochem Soc. 2016;163(9):A1872-80. doi: 10.1149/2.0411609jes

How to cite this article:
Keïta A, Yamegueu D, Sodiya K, Dumba DD. Q_{cycle}: A Field-Robust Metric for $LiFePO_4$ Battery Degradation Monitoring in Sahelian Solar Irrigation Systems. J Sustain Res. 2026;8(3): e260067. https://doi.org/10.20900/jsr20260067.